Vera C. Rubin Observatory
Systems Engineering

Impact of Optical Ghosts in Rubin Commissioning Data

Aashay Pai, Alex Drlica-Wagner, Lee S. Kelvin, and Joshua E. Meyers

SITCOMTN-173

Latest Revision: 2026-03-05

DRAFT

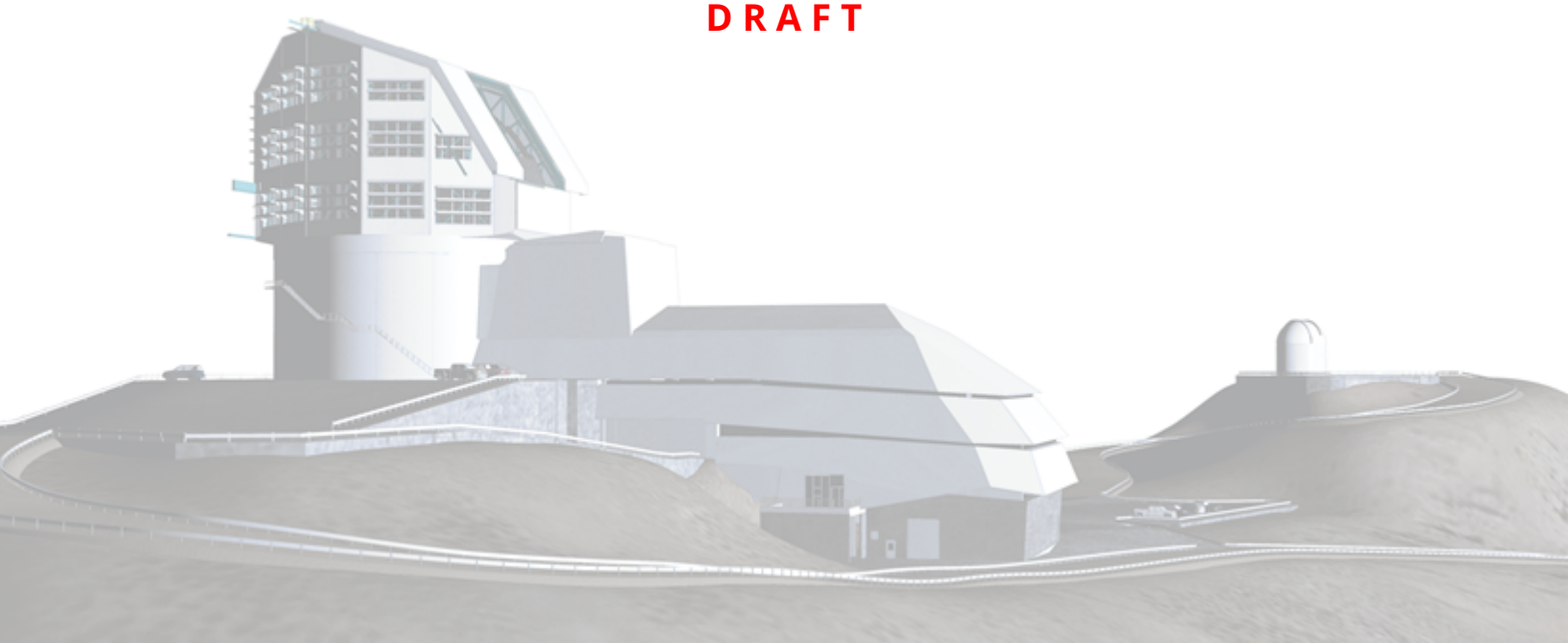

Abstract

Optical ghosts are image artifacts caused by successive reflections of light between optical surfaces such as lenses, filters, and detectors. These artifacts are unavoidable due to the nonzero reflectances of optical elements and are a major source of contamination for low-surface-brightness science. We use optical ray tracing simulations tuned to observations from LSST Commissioning to quantify the impact of optical ghosts on the LSST data. In particular, we find that $\sim 0.57\%$ of the LSSTCam focal plane is impacted by optical ghosts when averaged across all bands.

Change Record

Version	Date	Description	Owner name
1	YYYY-MM-DD	Unreleased.	Pai

Document source location: `https://github.com/lsst-sitcom/sitcomtn-173`

Contents

Impact of Optical Ghosts in Rubin Commissioning Data

1 Introduction

Optical ghosts are spurious reflections that appear in optical imaging systems as a result of multiple reflections of light off the optical elements in the system. Although ghosts are created by all astronomical sources, most of them are undetectable and have a negligible impact on the image. However, ghosts produced by bright stars can be quite impactful even if the reflectances of the optical elements are small ($\sim 1\%$) because the total number of photons from these stars are quite large. Figure 1 shows an example of optical ghosts created by a bright star in the top right corner of the LSST Camera focal plane during commissioning of the Vera C. Rubin Observatory.

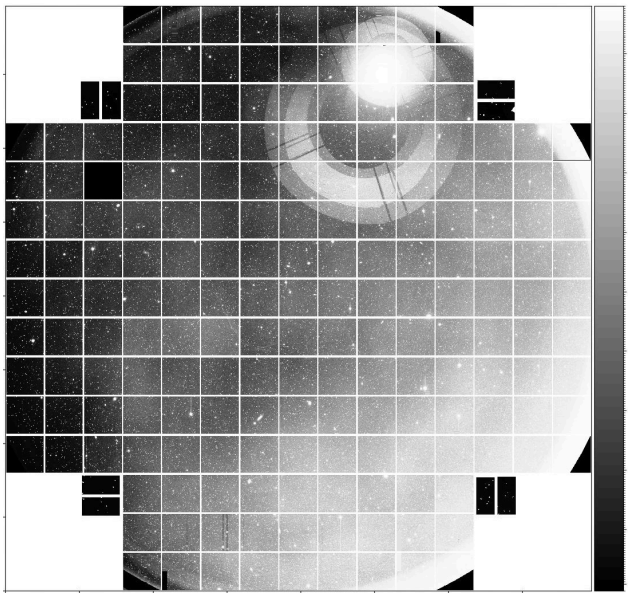

FIGURE 1: Post-ISR image of the LSSTCam focal plane (visit=2025110500406; band=*i*) with optical ghosts created by a bright star in the top right corner.

Ghosts produced by bright stars often pose challenges to sky background estimation and photometric measurements. They are also sources of contamination for low-surface-brightness science. Measuring the area of the focal plane impacted by these artifacts is therefore crucial to assess the impact on these science cases.

The LSST System Requirement[1] on the impact of optical ghosts states that the: "Percentage

[1] OSS Requirements: `https://docushare.lsst.org/docushare/dsweb/Get/LSE-30`; LSR Requirements: `https://`

of image area that can have ghosts with surface brightness gradient amplitude of more than $1/3$ of the sky noise over 1 arcsec shall be less than 1%". The wording of these requirements was intentionally left vague to allow subsequent groups to define it as appropriate. We opt to define it as the total area of the focal plane containing a ghost with a flux-to-sky-noise ratio exceeding a value of 1/3 on any detector. In order to satisfy this requirement, this value should not exceed 1%. We also assume that this requirement applies to the ensemble of visits, as opposed to every individual visit.

Measuring the fluxes of the ghosts with on-sky data to estimate the ghost flux-to-sky-noise ratio is challenging. Uneven flat-fielding during commissioning led to gradients in the mean sky counts across the focal plane, changing the baseline of the brightness of the ghosts from one side to the other. Most of the prominent ghosts were also found to be spatially degenerate, with some ghosts fully overlapping others. This made fitting the amplitude of each individual ghost difficult. To circumvent these challenges, we chose instead to calculate the expected impact of ghosts using simulations that were calibrated to commissioning data.

2 Methods

This section describes the steps used to estimate the ghost-impacted area for an individual LSSTCam visit.

2.1 Bright Stars

We retrieve all stars in the boresight from the Yale Bright Star Catalog Hoffleit & Warren (1991). We transform the V-band magnitudes of the bright stars to DES magnitudes following the procedure described in Appendix B of Abbott et al. (2021), which are then transformed again from DES to predicted LSST magnitudes following the prescription of Ferguson et al. (DMTN-277). We use the transformation equations listed in Eq. 1 to transform the magnitudes of the stars using the V magnitude and the $B - V$ color to DES magnitudes. These transformations are valid for $-0.2 < B - V \leq 2.2$.

docushare.lsst.org/docushare/dsweb/Get/LSE-29

$$
\begin{aligned}
g_{DES} &= V + 0.496(B - V) - 0.07 \\
r_{DES} &= V - 0.543(B - V) + 0.128 \\
i_{DES} &= V - 1.04(B - V) + 0.312 \\
z_{DES} &= V - 1.302(B - V) + 0.417 \\
Y_{DES} &= V - 1.416(B - V) + 0.504
\end{aligned}
\tag{1}
$$

To transform from DES to LSST, we use transformation equations derived using The Monster Ferguson et al. (DMTN-277). We are unable to use this sequence of transformations to generate predicted LSST u magnitudes as we did not have the transformation equations from the DECam u to LSSTCam u. In this case, we use the V magnitudes instead of the transformed LSST u magnitudes. We use the V band magnitude for all star magnitudes that we were unable to transform to LSST magnitudes.

2.2 Simulations

We use the `Batoid` Python package Meyers (2025) to generate simulated optical ghosts from bright stars in a particular visit.

2.2.1 Pipeline

Figure 2 shows a flowchart of the pipeline used to generate morphology, flux, and surface brightnesses of ghosts. The optical reflectances of the filters and lenses in the simulation were set to the values produced by the systems engineering simulations[2]. The bright stars were initialized into the simulation using the `preliminary_visit_image.wcs` object. The rays were then propagated through the full optical model. The flux of each ghost was converted from arbitrary flux units in `Batoid` to instrumental flux using Eq. 2, where f_i is the instrumental flux of a particular ghost, ϕ_{tot} is the total flux of all ghosts in arbitrary flux units, $\phi_\star$ is the flux of the star in arbitrary flux units and $f_\star$ is the instrumental flux of the star. $f_\star$ is calculated by converting the magnitude of the star in the LSST band to instrumental fluxes using the `preliminary_visit_image.photoCalib` object. Figure 3 shows the stacked optical ghosts produced by the simulation for visit 2025110500406.

[2] `https://github.com/lsst-pst/syseng_throughputs/blob/main/notebooks/Components.ipynb`

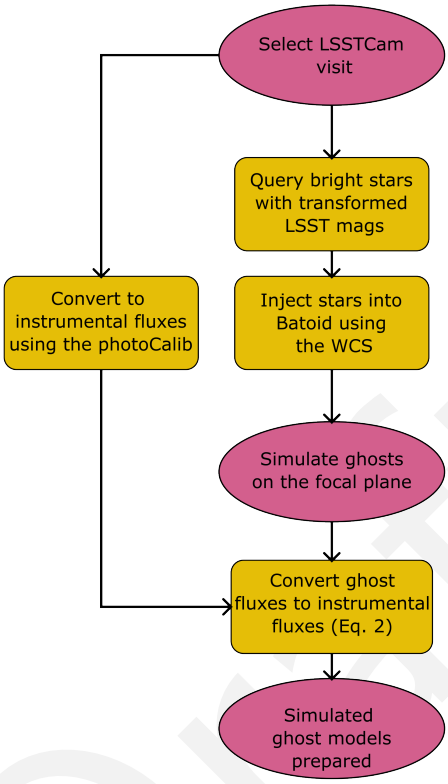

FIGURE 2: Flowchart showing the procedure used to generate optical ghost templates and surface brightness estimates.

$$f_i = \frac{\phi_i}{\phi_{tot} + \phi_\star} f_\star \tag{2}$$

2.2.2 Ghost Nomenclature & Morphology

In this technote, ghosts are labeled by the two optical elements that created them, ordered by the sequence of reflections. 'L#' stands for lens (# corresponds to the lens number which can be 1, 2 or 3), 'F' for filter, and 'D' for detector. The 1 or 2 at the end of each alphanumeric sequence denotes the surface of the optical element that the ray bounced off of. For example, the 'L31-F2' ghost was created due to the reflection of rays from the first surface (entrance) of L3 and again from the second surface (exit) of the Filter.

The ten most commonly occurring ghosts are: F2-F1, L32-F1, L32-F2, L31-F1, L31-F2, L32-L31, D-F1, D-F2, D-L31, D-L32. The F2-F1 ghost is the smallest and most stable with respect to

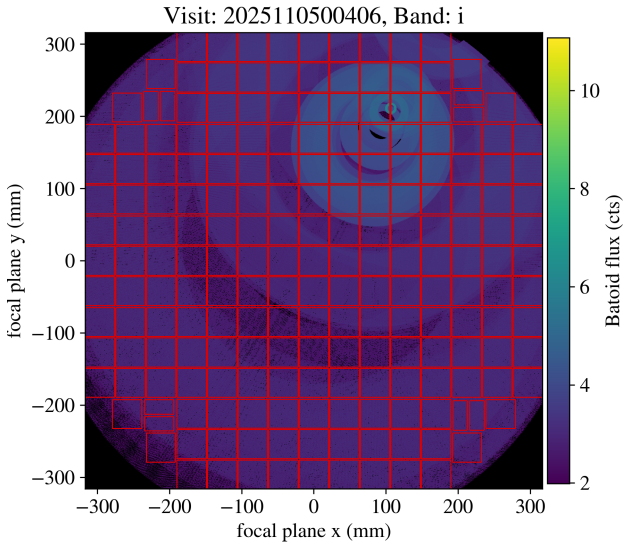

FIGURE 3: Stacked simulated ghosts produced by a `Batoid` simulation using the procedure delineated in Section 2.2.1.

position the focal-plane, while the D-F1 & D-F2 ghosts are the biggest and have the largest changes in ellipticity as the star moves off-axis.

Figure 4 shows an example LSSTCam visit with optical ghosts from Alpha Cen, along with a few of the simulated ghosts labeled by the optical elements responsible for creating them, their size, and the fraction of stellar flux that contributes to them.

2.3 Measuring the Impacted Area

To measure the impacted area as defined by our interpretation of the system requirement, we first generate individual ghost models using the algorithm in Section 2.2. For each individual ghost, the ghost area (in pixels) and the total ghost flux (in counts) is calculated per detector. The surface brightness of the ghost (S_i) is then calculated by dividing the total ghost flux per detector ($f_{tot,i}$) by the ghost area per detector (A_i), in units of counts per pixel as shown in Eq. 3. Here, i labels the detector number.

$$S_i = \frac{f_{tot,i}}{A_i} \tag{3}$$

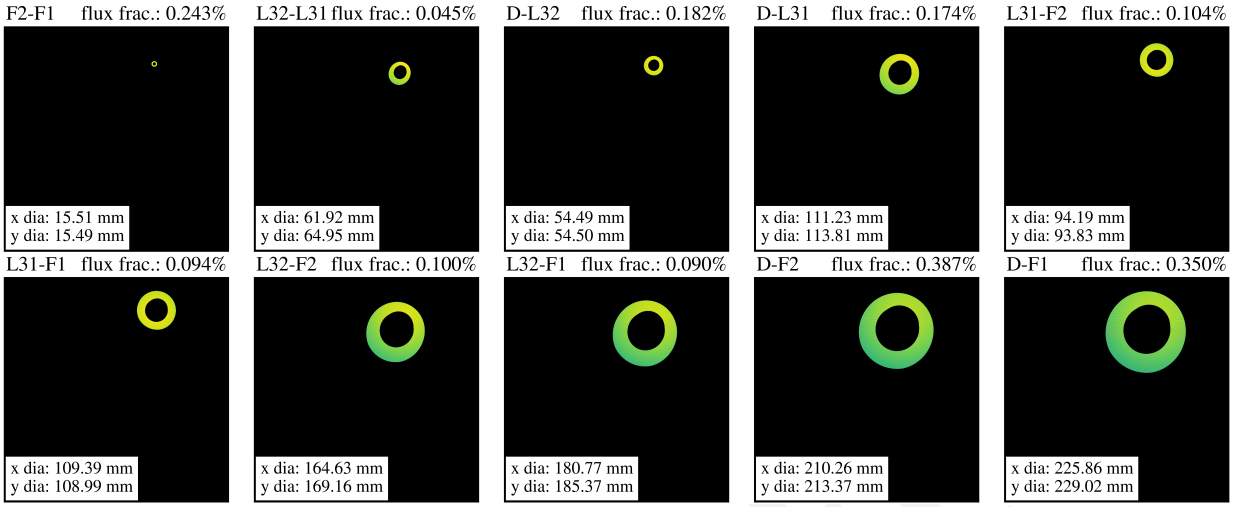

FIGURE 4: The ten most commonly occurring ghosts mentioned in Section 2.2.2 from the stacked simulation in Fig. 1. Each ghost is labelled by the pair of optical elements that the ray reflected off of, the fraction of stellar flux that contributed to the ghost and the x and y diameter.

The median measured sky noise per detector is queried for the visit through the LSSTCam ConsDB Lim (DMTN-227). We calculate the ratio of the ghost surface brightness to the sky noise. If this ratio exceeds $1/3$, the ghost area is marked as "impacted". Repeating this process for each ghost and accounting for ghost overlap gives us the final area of the focal plane that is impacted by ghosts. Figure 5 shows the area impacted by ghosts measured for visit 2025110500406. The impacted area is $1.19\,\mathrm{deg}^2$, which is 9.65% of the total focal plane area.

2.3.1 Impacted Area Statistics

We run the pipeline on two datasets to produce an estimate for the "usual" case and "worst" case ghost-impacted area. We used the weekly 37 intermittent DRP as the "usual" scenario to represent the LSST wide-fast-deep survey. The DRP covers a $30^\circ \times 20^\circ$ region with a centroid RA, Dec. $\sim (311.45^\circ, -18.43^\circ)$. We ran the pipeline above to measure the ghost-impacted area of the focal plane on ~3100 visits in the DRP. For the "worst" case estimate, we ran our pipeline on 20 visits in each band (except y, for which 20 visits with severe ghosting could not be identified) that were selected visually to contain large amounts of ghosting. Figure 6 shows that the ghost-impacted area in the DRP averaged over all bands and visits is 0.57%. When separated by band, the average impacted area in u is the highest at $\sim 8\%$ and smallest in r ($\sim 0.2\%$) and i ($< 0.1\%$). The anomalously high value in u is likely due to the lower sky background in the u-band. Table 2.3.1 shows the total impacted area and surveyed area in each band in the w37

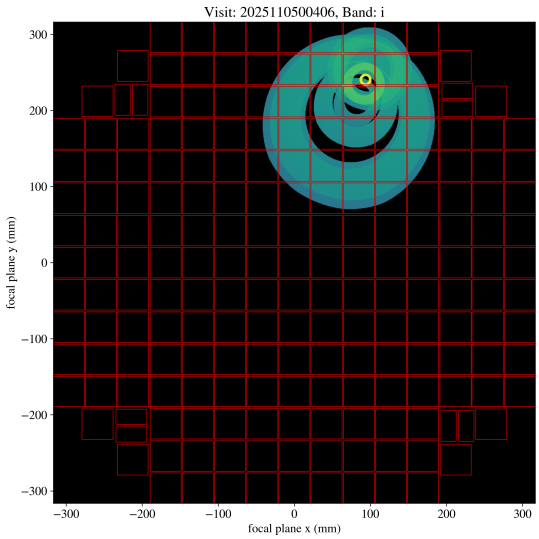

FIGURE 5: Area of the focal plane marked as impacted by optical ghosts in green for LSSTCam visit 2025110500406. For this particular visit, we find the area significantly impacted by ghosts to be 9.65% of the total focal plane area.

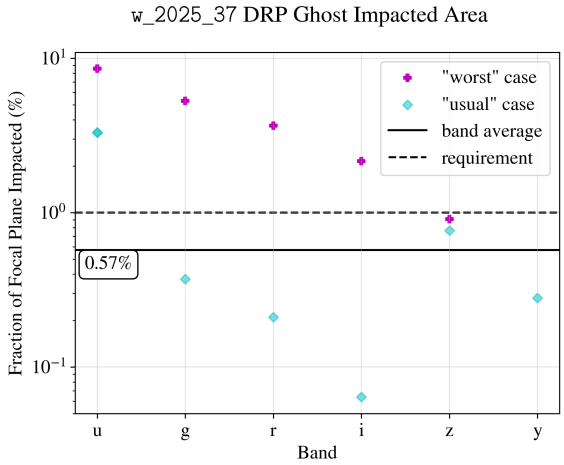

FIGURE 6: Area of the focal plane impacted by ghosts separated by band in the w37 DRP (cyan) and in a set of highly-ghosted visits in all bands except y (magenta). The impacted area in the DRP is 0.57% when averaged across all bands. The highest contribution is from u and the lowest from i.

intermittent DRP.

We also simulate a single star with different magnitudes at various off-axis positions on the focal plane to plot the impacted area as a function of star magnitude in Fig. 7. The left panel

Band	Impacted Area [deg^2]	Surveyed Area [deg^2]
u	68.95	2225.91
g	14.01	4897.00
r	9.94	6084.15
i	4.04	9719.80
z	33.56	8668.68
y	7.96	6603.53

TABLE 1: w37 DRP ghost-impacted and surveyed sky area separated by band.

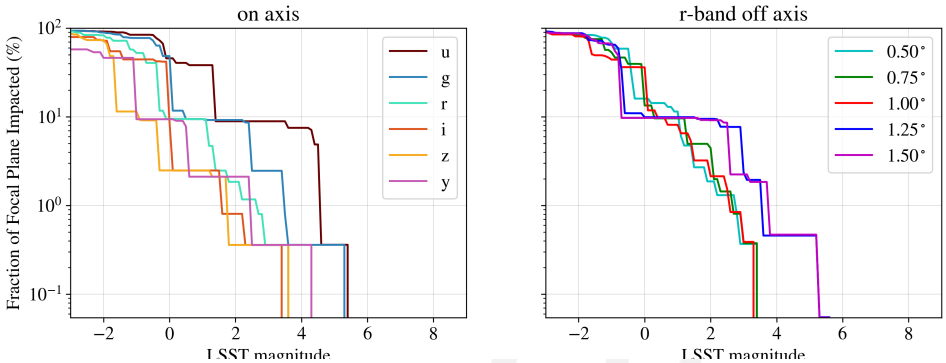

FIGURE 7: (Left) Fraction of the focal plane impacted by optical ghosts as a function of star magnitude for a single on-axis simulated star. (Right) The r-band impacted area as a function of star magnitude for different off-axis positions of the simulated star.

shows the impacted area as a function of the magnitude of an on-axis bright star separated by band, and the right panel shows the weak dependence of the impacted area on the star's offset angle relative to the boresight.

We use the left panel from Fig.7 as a look-up table to generate a sky map of the impacted area from all the stars in the Yale Bright Star catalog, assuming that each star was observed on-axis. We use the nominal zeropoints and dark sky counts from SMTN-002 Jones (SMTN-002) to calculate the sky noise in each band. We also assume that the exposure times for each band were 30 s. These maps for each band are shown in Fig. 8.

Note that in these maps, the impacted area from each bright star within the same pixel is simply added. This leads to a slight over-counting of the impacted area, as stars that are close to each other can produce overlapping ghosts, changing the total impacted area of the two stars from a simple sum to a union of the individual impacted areas.

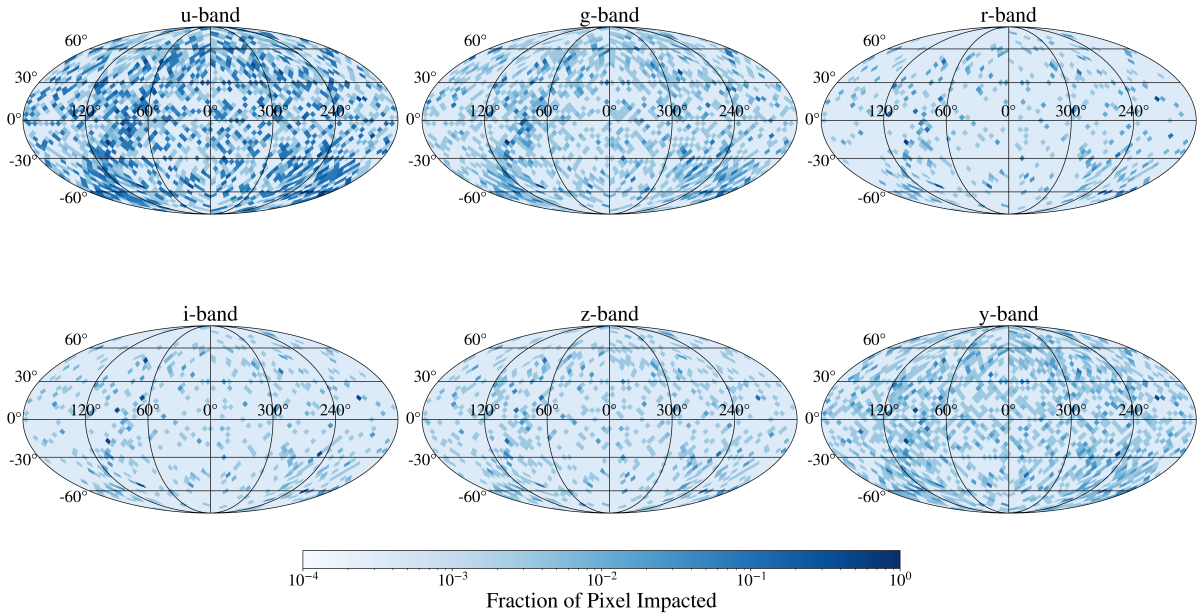

FIGURE 8: Sky maps showing the fraction of ghost-impacted area in each pixel from the stars in the Yale Bright Star Catalog, separated by band using the simulations in Fig. 7.

3 Conclusions

We have presented a simulation-based framework for quantifying the impact of optical ghosts on LSSTCam imaging, motivated by the need to assess compliance with the LSST system requirements.We combine the Yale Bright Star Catalog, empirically calibrated magnitude transformations, and optical ray-tracing simulations using `Batoid`, to estimate both the morphology and surface brightness of the dominant ghosts and measure the resulting ghost-impacted area on the focal plane.

Applying this framework to ~3100 visits from the w37 intermittent DRP, we find that the average fraction of the LSSTCam focal plane significantly impacted by ghosts is 0.57% when averaged across all bands. This value is below the 1% threshold specified by the LSST system requirement when interpreted in an ensemble-averaged sense. The impacted area exhibits strong band dependence, with the largest contributions occurring in the u band due to its lower sky background, and minimal impact in the r and i bands. It The impacted area is also heavily dependent on the field being observed, as ndividual visits containing very bright stars can show substantially larger impacted fractions.

We further explored the dependence of ghost-impacted area on stellar magnitude and off-axis position, finding that star brightness is the dominant driver of ghost impact, with only a weak dependence on field angle. Using these results, we constructed all-sky maps of expected ghost-impacted area based on the Yale Bright Star Catalog.

Overall, our results demonstrate that optical ghosts are a non-negligible source of contamination for low-surface-brightness science in LSST, particularly in the presence of very bright stars.

A Acknowledgements

This material is based upon work supported in part by the National Science Foundation through Cooperative Agreements AST-1258333 and AST-2241526 and Cooperative Support Agreements AST-1202910 and AST-2211468 managed by the Association of Universities for Research in Astronomy (AURA), and the Department of Energy under Contract No. DE-AC02-76SF00515 with the SLAC National Accelerator Laboratory managed by Stanford University. Additional Rubin Observatory funding comes from private donations, grants to universities, and in-kind support from LSST-DA Institutional Members.

B References

Abbott, T.M.C., Adamów, M., Aguena, M., et al., 2021, ApJS, 255, 20 (arXiv:2101.05765), doi:10.3847/1538-4365/ac00b3, ADS Link

[DMTN-277], Ferguson, P.S., Rykoff, E.S., Carlin, J.L., Saunders, C., Parejko, J.K., 2025, *The Monster: A reference catalog with synthetic ugrizy-band fluxes for the Vera C. Rubin observatory*, Data Management Technical Note DMTN-277, NSF-DOE Vera C. Rubin Observatory, URL https://dmtn-277.lsst.io/, doi:10.71929/rubin/2583688

Hoffleit, D., Warren, W.H., 1991, *The Bright Star Catalogue, 5th Revised Edition (Preliminary Version)*, Yale University Observatory, New Haven, CT, URL https://vizier.cds.unistra.fr/viz-bin/VizieR?-source=V/50,
Yale University Observatory, 5th Revised Edition

[SMTN-002], Jones, R.L., 2025, *Calculating LSST limiting magnitudes and SNR*, Simulations Team Technical Note SMTN-002, NSF-DOE Vera C. Rubin Observatory, URL https://smtn-002.lsst.io/

[DMTN-227], Lim, K.T., 2025, *The Consolidated Database of Image Metadata*, Data Management Technical Note DMTN-227, NSF-DOE Vera C. Rubin Observatory, URL https://dmtn-227.lsst.io/, doi:10.71929/rubin/2586436

Meyers, J.E., 2025, Batoid: a c++-backed python optical ray-tracer (version 0.8.0), https://github.com/jmeyers314/batoid, doi:10.5281/zenodo.14814750

C Acronyms

Acronym	Description
AST	NSF Division of Astronomical Sciences
AURA	Association of Universities for Research in Astronomy
B	Byte (8 bit)
DE-AC02	Department of Energy contract number prefix
DECam	Dark Energy Camera
DES	Dark Energy Survey
DMTN	DM Technical Note
DRP	Data Release Processing
ISR	Instrument Signal Removal
L3	Lens 3
LSE	LSST Systems Engineering (Document Handle)
LSR	LSST System Requirements; LSE-29
LSST	Legacy Survey of Space and Time (formerly Large Synoptic Survey Telescope)
LSST-DA	LSST Discovery Alliance
LSSTCam	LSST Science Camera
OSS	Observatory System Specifications; LSE-30
RA	Rapid Analysis
SI	System and Information Integrity
SLAC	SLAC National Accelerator Laboratory